

# AIP | Review of Scientific Instruments

## Ferrule-top nanoindenter: An optomechanical fiber sensor for nanoindentation

D. Chavan, T. C. van de Watering, G. Gruca, J. H. Rector, K. Heck et al.

Citation: *Rev. Sci. Instrum.* **83**, 115110 (2012); doi: 10.1063/1.4766959

View online: <http://dx.doi.org/10.1063/1.4766959>

View Table of Contents: <http://rsi.aip.org/resource/1/RSINAK/v83/i11>

Published by the [American Institute of Physics](http://www.aip.org).

---

### Additional information on Rev. Sci. Instrum.


Journal Homepage: <http://rsi.aip.org>

Journal Information: [http://rsi.aip.org/about/about\\_the\\_journal](http://rsi.aip.org/about/about_the_journal)


Top downloads: [http://rsi.aip.org/features/most\\_downloaded](http://rsi.aip.org/features/most_downloaded)

Information for Authors: <http://rsi.aip.org/authors>

## ADVERTISEMENT



**Does your research require low temperatures? Contact Janis today. Our engineers will assist you in choosing the best system for your application.**



- 10 mK to 800 K
- Cryocoolers
- Dilution Refrigerator Systems
- Micro-manipulated Probe Stations
- LHe/LN<sub>2</sub> Cryostats
- Magnet Systems

[sales@janis.com](mailto:sales@janis.com)   [www.janis.com](http://www.janis.com)  
**Click to view our product web page.**

## Ferrule-top nanoindenter: An optomechanical fiber sensor for nanoindentation

D. Chavan, T. C. van de Watering, G. Gruca, J. H. Rector, K. Heeck, M. Slaman, and D. Iannuzzi

*Vrije Universiteit and LaserLaB, Amsterdam, The Netherlands*

(Received 2 August 2012; accepted 26 October 2012; published online 27 November 2012)

Ferrule-top probes are self-aligned all-optical devices obtained by fabricating a cantilever on the top of a ferruled optical fiber. This approach has been proven to provide a new platform for the realization of small footprint atomic force microscopes (AFMs) that adapt well to utilization outside specialized laboratories [D. Chavan *et al.*, *Rev. Sci. Instrum.* **81**, 123702 (2010); **82**, 046107 (2011)]. In this paper we now show that ferrule-top cantilevers can be also used to develop nanoindenters. Our instrument combines the sensitivity of commercial AFM-based indentation with the ease-of-use of more macroscopic instrumented indenters available today on the market. Furthermore, the all-optical design allows smooth operations also in liquids, where other devices are much more limited and often provide data that are difficult to interpret. This study may pave the way to the implementation of a new generation user-friendly nanoindenters for the measurement of the stiffness of samples in material sciences and medical research. © 2012 American Institute of Physics. [<http://dx.doi.org/10.1063/1.4766959>]

### I. INTRODUCTION

Depth sensing indentation, as proposed by Oliver and Pharr,<sup>1</sup> is currently recognized as one of the most powerful techniques for the mechanical characterization of compliant, elastic-plastic materials at the nanoscale. The technique relies on the possibility to indent the sample of interest with a tip of known geometry while simultaneously recording the load applied and the penetration depth. The two most common categories of instruments used to perform this kind of indentation testing are the commercial instrumented indenter<sup>2</sup> and the atomic force microscope (AFM).<sup>3</sup> In spite of their success, both the instruments come with some drawbacks. Most instrumented indenters are typically equipped with a stiff force sensor that limits the overall force resolution to a few microNewtons. Moreover, if the sample is submerged in a liquid medium, the force due to the water meniscus on the shaft of the indenter makes the indentation data analysis more complicated.<sup>4</sup> On other hand, AFMs offer better force resolution (below nanoNewtons)—an advantage that has been widely used in several experiments focused on soft polymers,<sup>5,6</sup> tissues,<sup>7,8</sup> and cells.<sup>9,10</sup> Nevertheless, the use of AFMs outside research laboratories is hampered by the complexity of the instrument. Furthermore, in order to perform AFM indentation in a liquid, one needs to mount the sample inside a specially designed fluid chamber, which limits the sample size to a few squared centimeters and increases the complexity of the apparatus even more.

In this paper, we introduce a new indentation instrument that can operate in air and in liquids with a force resolution comparable to the one achieved by AFMs while maintaining the ease of use of instrumented indenters. Our indenter is based on a force probe obtained by carving a cantilever on the top of a glass ferrule that hosts an optical fiber for readout purposes—a design also known as *ferrule-top* technology.<sup>11</sup> We have recently demonstrated that a ferrule-top cantilever

probe equipped with a sharp tip can be used to develop user-friendly AFMs for high resolution images in air, vacuum, low temperatures, and liquids.<sup>12,13</sup> Here, we show that ferrule-top AFMs can be also used as high resolution, plug-and-play instruments for Young modulus measurements of elastic compliant materials, both in air and liquids.

### II. EXPERIMENTAL DETAILS

#### A. Ferrule-top probe fabrication

Ferrule-top cantilevers are obtained by carving a cantilever on top of a glass ferrule. Figure 1 shows the most important steps of the fabrication process.

The building block is a 3 mm × 3 mm × 7 mm borosilicate glass ferrule with a 50 μm and a 125 μm bore holes (Fig. 1(i)). The glass ferrule is mounted on a ps-laser ablation system (Optec System with Lumera Laser source) to carve a central ridge and a lateral groove (Fig. 1(ii)). The latter is designed to host a fiber terminated with a spherical tip, which will be eventually used to indent the sample. The spherical indentation tip is obtained by melting a chemically etched optical fiber with a high current spark. The radius of the sphere can be adjusted by properly setting the etching time, and, hence, the radius of the fiber. This technique proves to be highly reproducible and to provide an optically smooth spherical tip. Alternatively, sharp conical indentation tips (radius ~100 nm) can be obtained by etching a special highly doped germanium fiber in buffered HF.<sup>14</sup> Figure 2 shows the scanning electron microscope images of the tips fabricated with the methods described above. In this study, which is focused on indentation of compliant soft materials, we only use large radius spherical indentation tips (Figs. 2(c) and 2(d)).

After the tipped fiber is glued in the groove (Fig. 1(iii)), the ferrule is mounted on the laser ablation system to perform the undercut and release the cantilever (Fig. 1(iv)). The

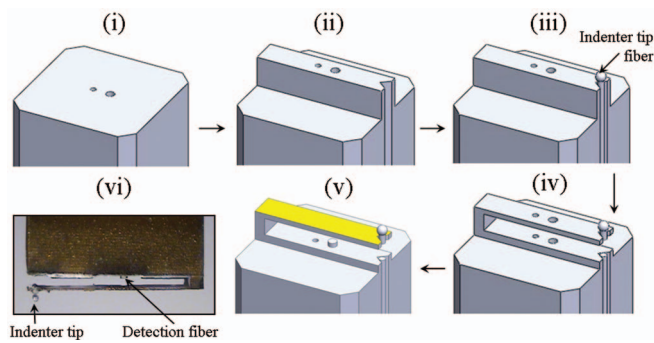


FIG. 1. Fabrication process for ferrule-top indenter probes (not to scale): we refer the reader to the main text for a detailed explanation of the steps illustrated.

125  $\mu\text{m}$  hole in the cantilever is filled by UV curable glue (Norland 68) followed by sputtering of chromium (10 nm) and gold (50 nm). Finally, a cleaved single mode optical fiber (Corning SMF28) is slid into the 125  $\mu\text{m}$  bore hole (Fig. 1(v)). The other end of this fiber is connected to an optical fiber interferometer readout, which will be described later in the text. The spring constant of the cantilever largely depends on the geometrical dimensions chosen during the fabrication process. For the experiments reported in this paper, we used three ferrule-top cantilever probes, whose characteristics are reported in Table I. The nominal stiffness of the cantilever was calculated from the dimensions of the cantilever. Note that Probe-1 and -3 were fabricated according to Fig. 1. Probe-2 was obtained by first cutting the ferrule to a 3 mm  $\times$  1.7 mm  $\times$  7 mm initial block, and then following the very same process illustrated in Fig. 1, with a resulting cantilever that is half the length as in the case of Probe-1 and -3.

## B. Experimental setup

Figure 3 shows a sketch of the ferrule-top indenter developed for this experiment. The ferrule-top indenter probe is

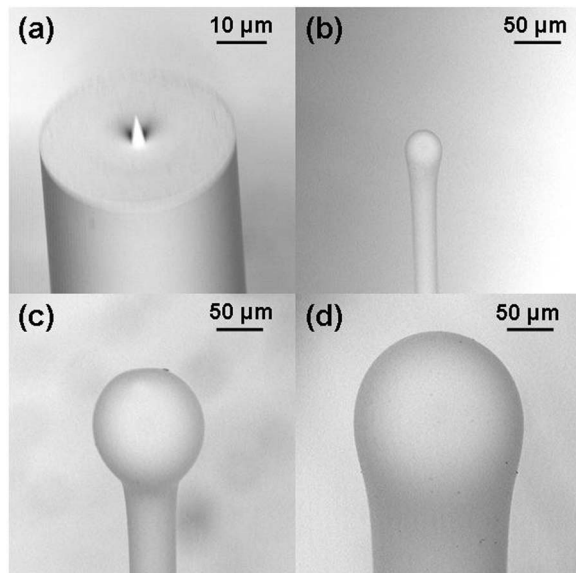


FIG. 2. Indentation tips of different sizes obtained by modifying optical fibers.

TABLE I. Ferrule-top indenter probes used for indentation experiments.

	Indenter shape	Indenter tip radius ( $\mu\text{m}$ )	Nominal cantilever stiffness (N/m)
Probe-1	Sphere	55	31
Probe-2	Sphere	80	66
Probe-3	Sphere	80	34

glued to a small piece of iron, which is attached to a magnet anchored to a coarse z-positioner. The sample is mounted on a closed-loop z-piezoelectric translator (P-611.ZS, PI GmbH) equipped with an integrated strain gauge sensor and controlled by a closed-loop servo controller (E-665.SR, PI GmbH). This translator is used to bring about the desired indentation stroke of up to 100  $\mu\text{m}$ , with 2 nm resolution and nonlinearity of 0.1%. To give the user the possibility to indent different points of the sample, the z-piezoelectric translator is screwed on an xy-translation stage (PI GmbH). To reduce acoustic and seismic noise, the entire setup is mounted on an active vibration isolation stage (Nano-20, Accurion GmbH) housed inside an anechoic box.

The setup is controlled via a LabVIEW program that allows the user to select the desired depth and speed of the indentation stroke. The data acquired by the program during the measurement are analyzed using a separate in-house developed data analysis program.

## C. Readout

The readout connected to the other end of the ferrule-top probe measures the deflection of the cantilever during indentation via Fabry-Pérot interferometry (see Fig. 4).

A monochromatic light source is connected to a 90/10 coupler. The 10% arm of the coupler is connected to the ferrule-top probe and the 90% arm is not in use. A photodiode (Newport Inc.) aligned with the forth port of the coupler is then used to measure the intensity of the light reflected

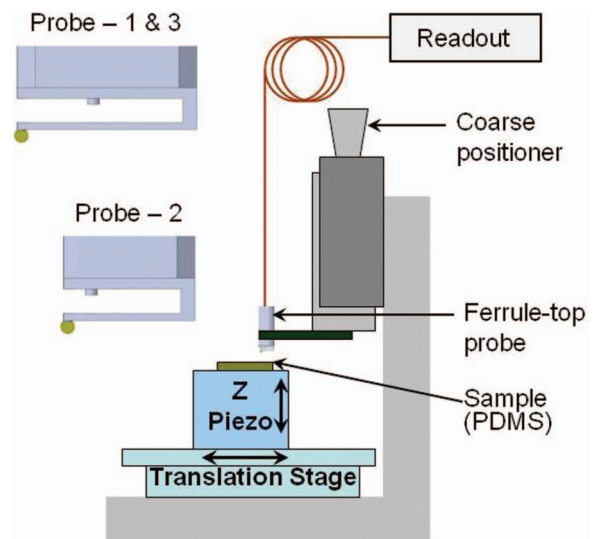


FIG. 3. Schematic view of the ferrule-top nanoindenter setup.

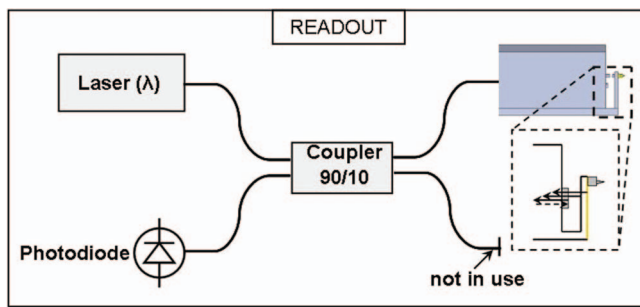


FIG. 4. Readout for ferrule-top cantilever probes.

back from the probe head, which is the result of the interference between the light reflected at fiber-to-gap interface, the light reflected by gap-to-cantilever interface, and the light reflected at the cantilever-to-metal interface. The amplitude of this signal is given by<sup>15</sup>

$$W(d) = W_0 \left[ 1 + V \cdot \cos \left( \frac{4\pi d}{\lambda} + \phi_0 \right) \right], \quad (1)$$

where  $d$  is the separation between the fiber-to-gap and the gap-to-cantilever interfaces,  $\phi_0$  is a constant phase shift that only depends on the geometry of the cantilever,  $\lambda$  is the wavelength of the source,  $W_0$  is the midpoint interference signal, and  $V$  is the fringe visibility.

Before the start of the indentation experiment, it is first convenient to adjust the interference signal  $W_0$  at the midpoint of the fringe, i.e., at quadrature. Using this setting, the readout provides a linear signal both when the cantilever bends backwards during forward indentation and when the cantilever, trapped by contact forces, bends forward during the retraction of the indenting tip. The midpoint can be achieved by either tuning the dimensions of the Fabry-Pérot cavity or by tuning the wavelength of the light source. Due to the limitations of the fabrication process, the only viable solution is to tune the wavelength of the light source. The light source thus consists of a broadband superluminescent diode (SLD) (SM Benchtop SLD Source, 1550 nm central wavelength, 22 mW, 45 nm bandwidth, Thorlabs GmbH) connected to a manual fiber optic tunable filter (Agiltron Inc.), which can be tuned to reach quadrature. The advantages of this configuration are shown in Fig. 5, where we report the interference fringe due to bending of the cantilever upon indenting a glass as recorded with two different wavelengths: one corresponding to the midpoint ( $\lambda_1$ ) and another one corresponding to an interference point close to a maximum of interference ( $\lambda_2$ ).

To translate the detector output (in volts) to deflection of cantilever  $d_c$  (in nanometers), one needs to measure the deflection sensitivity (nm/V). This proportionality constant can be readily measured by indenting a very stiff sample (e.g., a piece of glass), so stiff that the indentation depth can be safely set to zero. Under this assumption, the indenter tip deflects the same amount as the close-loop piezo movement. From the slope of the linear part of the fringe (shown in Fig. 5 by the dashed line), one can thus extract the deflection sensitivity of that probe for the given laser power and detector gain. It is clear that the value obtained via this calibration measure-

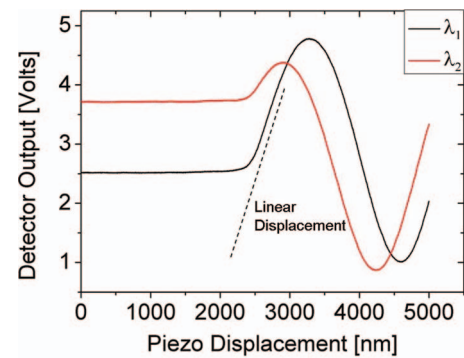


FIG. 5. Readout signal observed while indenting a glass sample with a ferrule-top indenter. The two lines correspond to two different wavelengths of the light source mounted in the readout. The graph is meant to illustrate the advantages (in terms of signal linearity) of working close to quadrature ( $\lambda_1$ ) rather than close to a maximum of interference ( $\lambda_2$ ).

ment is only viable to analyze data in the linear part of the interference fringe, which corresponds to about one fourth of  $\lambda$  ( $\sim 387$  nm). This value is sufficiently large in most indentation experiments. The deflection sensitivity for Probe-1, -2, and -3 was calculated to be 327 nm/V, 99 nm/V, and 465 nm/V in air, respectively, and 478 nm/V for Probe-1 in water. The small difference between the values measured for Probe-1 and Probe-3 are due to the fact that the deflection sensitivity depends on the length of the Fabry-Pérot cavity (which can be fixed, during fabrication, only within approximately 100  $\mu\text{m}$ ), the reflectivity of the cantilever (which cannot be entirely controlled with the current manufacturing process), and the setting of the readout (laser power and detector gain, which are often tuned to optimize the output signal to the experimental conditions). The larger difference in deflection sensitivity observed for Probe-2, on the other hand, can be ascribed to the different geometry of the probes (see Fig. 3). In Probe-2, in fact, the cantilever end hangs over the central detection fiber, while in Probe-1 and -3 it runs over the whole width of the ferrule, with the detection fiber aligned to the middle deflection point. This geometrical feature has of course a dramatic effect on the deflection sensitivity.

The force resolution of our setup is determined by the random fluctuations of the length of the Fabry-Pérot cavity formed between the detection fiber and the cantilever, which are induced by the coupling of acoustic and mechanical vibrations into the probe. Those fluctuations produce the dominant part of the noise at the output of the readout (expressed in V) that, multiplied by the deflection sensitivity (expressed in m/V) and by the spring constant of the cantilever (expressed in N/m), provides the force noise. For our setup, the rms noise in air at the output of the readout, sampled at a 1000 sample/s, is approximately 2 mV. Sampling at higher bandwidth (10 kHz) does not result in a measurable higher rms, as expected for a noise spectrum dominated by low frequency components. For a typical ferrule-top probe (deflection sensitivity  $\sim 300$  nm/V), this rms value corresponds to a cantilever deflection resolution of 0.6 nm, which, for a cantilever with spring constant  $\sim 30$  N/m, translates in a force sensitivity of 18 nN.



## D. Experimental procedure and working principle

Indentation was performed on PDMS (polydimethylsiloxane, Sylgard-184, Dow Corning, Inc) samples of two different moduli, obtained by mixing the elastomer and the cross linking agent in ratios of 10:1 and 20:1, respectively. The two mixtures (10:1 and 20:1) were allowed to degas for 30 min to remove air bubbles, and kept in a oven at 100 °C for 45 min to cure the PDMS before use. The thickness of the samples was in the order of 2 to 3 mm. Sample pieces of size 10 mm × 10 mm were cut and glued to a petri dish, which was mounted on top of the z-piezoelectric translator. Indentation curves were obtained with the following procedure. The probe was first brought close to the sample (PDMS) by the coarse positioner within a separation distance of few tens of microns. The sample was then moved by the z-piezoelectric translator at a rate of 1 μm/s towards the probe until, after entering in contact with the indentation tip of the ferrule-top probe, it would have induced the cantilever to bend backwards for a few tens of nanometers. At the end of this procedure, the z-piezoelectric translator retracted the sample a few microns away from the indenting tip. This position was set as the initial vertical point of all the following indentation curves. Starting from this position, several different points of the sample (selected via the xy translational stage) were finally indented with a loading and unloading rate of 1 μm/s.

To test the ferrule-top indenter in liquids, we simply filled the petri dish with water. The probe was then lowered into the petri dish with the coarse positioner, and the indentation procedure was repeated following the same procedure as for the indentation in air, including the measurement of the deflection sensitivity at the start of the measurements.

From these indentation tests, the indentation depth ( $d_i$ ) can be obtained by subtracting the deflection of the cantilever measured by the interferometer ( $d_c$ ) to the piezo displacement ( $d_p$ ):

$$d_i = d_p - d_c. \quad (2)$$

The load applied during the indentation cycle is given by

$$P = k \cdot d_c, \quad (3)$$

where  $k$  is the stiffness of the cantilever as listed in Table I.

The raw indentation data acquired from the indentation program were further processed to estimate the Young's modulus following an algorithm that is explained in Sec. III. For the measurements in air, at least 15 indentation curves, obtained in different points of the sample, were considered for each probe (1, 2, and 3) and for each sample (10:1 and 20:1). Indentation in liquid was performed only with Probe-1, with 9 indentation curves for the 10:1 sample and with 8 curves for the 20:1 sample. The indentation spots were at least 0.5 mm apart from each other.

## III. RESULTS AND DISCUSSIONS

Hertzian contact mechanics<sup>16</sup> is a classical theory that can be used to quantitatively estimate the material properties of an elastic sample from indentation data. Following this theory, one can write the load  $P$  applied by the indenter in terms

of the reduced Young moduli of the indenting material  $E_1$  and of the indented material  $E_2$ :

$$P = \frac{4}{3} E^* R^{1/2} d_i^{3/2}, \quad (4)$$

where  $R$  is the indenter tip radius,  $d_i$  is the indentation depth, and  $E^*$  is the reduced modulus, which is given by

$$\frac{1}{E^*} = \frac{1 - \nu_1^2}{E_1} + \frac{1 - \nu_2^2}{E_2}, \quad (5)$$

where  $\nu_1$  and  $\nu_2$  are the Poisson's ratios of the indenting and of the indented materials, respectively. Hertz model applies only to fully elastic contacts with small indentation depths (as compared to the indenter radius) and no adhesive forces. However, during indentation of compliant materials, adhesive and capillary forces between the tip and the sample cannot be neglected. To take into account this effect, it is more appropriate to use either the Johnson-Kendall-Roberts (JKR)<sup>17</sup> or the Derjaguin-Muller-Toporov (DMT)<sup>18</sup> model. The JKR model predicts the indentation behavior of a soft material by a large indenter tip radius, whereas the DMT model predicts the indentation behavior of a stiffer material with a smaller indenter tip radius. To determine which of the two models is more appropriate, one can calculate the Tabor coefficient,<sup>19</sup> which is given by

$$\mu = \left( \frac{R \cdot \Delta\gamma^2}{E^* z_0^3} \right)^{1/3}, \quad (6)$$

where  $R$  is the indentation tip radius,  $\Delta\gamma$  is the work of adhesion,  $E^*$  is the reduced sample modulus, and  $z_0$  is the equilibrium separation between atoms. The DMT and JKR model can be safely applied for  $\mu < 0.1$  and  $\mu > 5$ . For  $0.1 < \mu < 5$  other models have been developed.<sup>20</sup>

In order to assess the value of the Tabor coefficient for our experimental conditions, we first need to estimate the value of  $\Delta\gamma$ . Figure 6 shows a typical load-versus-indentation curve obtained while indenting with Probe-1 the 10:1 PDMS sample.

The role of adhesive forces is quite evident, as it causes a deep minimum in the unloading curve. This minimum can be used to roughly estimate the work of adhesion according to

$$\Delta\gamma = -\frac{2 P_{adh}}{3 \pi R}, \quad (7)$$

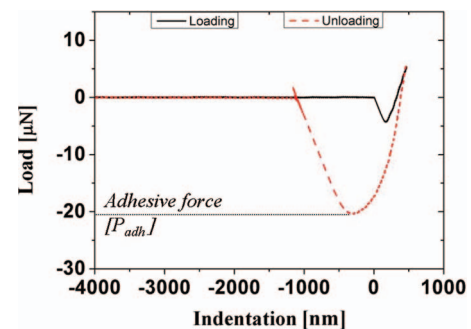


FIG. 6. Load versus indentation depth curves obtained while indenting the PDMS 10:1 sample with Probe-1.

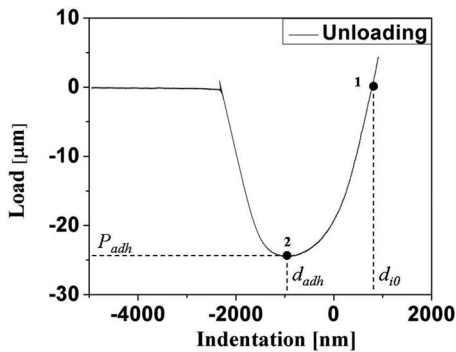


FIG. 7. Illustration of the 2-point analysis method.

where  $P_{adh}$  can be taken as the value of the minimum in the unloading curve. For  $P_{adh} \approx 20 \mu\text{N}$ ,  $R = 55 \mu\text{m}$ ,  $E \approx 5 \text{ MPa}$ , and  $z_0 \approx 0.5 \text{ nm}$ ,<sup>21</sup> one obtains  $\mu \approx 470 (\gg 5)$  which indicates that, for the analysis of this set of data, the JKR model is more appropriate. Similar results can be retrieved for all the other in-air experiments reported in this paper.

To simplify the analysis of the experimental curves, we have followed the JKR 2-point method,<sup>21,22</sup> which makes use of only two points of the unloading curve (see Fig. 7).

The first point (point 1 of Fig. 7) corresponds to the point where the unloading curve crosses the zero load line. This point gives the indentation depth for zero load ( $d_{i0}$ ). The second point (point 2 of Fig. 7) corresponds to the maximum adhesion point of unloading curve, which gives the negative adhesive load ( $P_{adh}$ ) and the negative indentation depth ( $d_{iadh}$ ). The values  $d_{i0}$ ,  $d_{iadh}$ , and  $P_{adh}$  obtained from the unloading part for each indentation curve, can be then used to calculate the sample modulus according to<sup>21</sup>

$$E^* = -\frac{3P_{adh}}{\sqrt{R}} \left[ \frac{3(d_{i0} - d_{iadh})}{1 + 4^{-2/3}} \right]^{-3/2}. \quad (8)$$

Table II shows the Young modulus of the two PDMS samples (10:1 and 20:1) as measured with the three probes. The modulus values measured by all the three probes are in good agreement with those published in the literature.<sup>23,24</sup> It is still important to stress that, by using the nominal value of the spring constant of the cantilever to convert cantilever bending into force, we may have introduced a significant systematic error. The validity of our method can then be checked by looking at the ratio between the Young modulus measured for the 10:1 sample and that measured for the 20:1 sample. This parameter gives the relative stiffness between the two samples, and is thus not affected by the systematic error discussed above. The modulus ratios measured by the three probes, also reported in Table II, show indeed good consistency between different experiments.

In Fig. 8 we report a representative load-versus-indentation curve obtained while indenting, with Probe-1, the 20:1 sample immersed in water. It is evident that the presence of water reduces adhesion and capillary effects to negligible levels.

Because of the absence of adhesive forces and residual impression, data obtained in water can be elaborated via the Hertz model (Eq. (1)). Following this procedure, we obtained

TABLE II. Result of the measurement of the reduced Young modulus of two PDMS samples with three different probes.

	PDMS (MPa) 10:1	PDMS (MPa) 20:1	Modulus ratio 10:1/20:1
Probe-1	$4.60 \pm 0.12$	$1.43 \pm 0.11$	3.21
Probe-2	$3.41 \pm 0.20$	$1.10 \pm 0.04$	3.10
Probe-3	$4.49 \pm 0.10$	$1.44 \pm 0.07$	3.12

a Young modulus of  $2.28 \pm 0.23 \text{ MPa}$  and  $0.95 \pm 0.21 \text{ MPa}$  for the 10:1 and 20:1 sample, respectively, with a modulus ratio of 2.40 (as measured with Probe-1; Probe-2, and Probe-3 were not used in water). The periodic noise pattern observed for indentation curves in liquid (see Fig. 8), has contribution from frequencies in the range of 32–52 Hz. We suspect this low frequency noise can arise from the mechanical vibrations sensed by the Fabry-Perot cavity.

The sample moduli and the modulus ratio calculated for indentations performed in liquid deviates appreciably from those measured for the same sample in air. Similar deviation in modulus values of PDMS measured in air and aqueous solution are reported earlier.<sup>24</sup> The origin of this effect is still not completely understood. Other factors that can influence the calculated sample modulus in air and water are surface roughness, surface contaminations, thermal drifts, deviation from actual tip geometry, variation in deflection sensitivity of the cantilever due to laser power variation, and nonlinearities of the piezoelectric scanner. This kind of problems is common to other techniques, and their analysis goes beyond the scope of this paper. This work should in fact not be taken as an attempt to provide a metrological assessment of the mechanical properties of PDMS but more as a demonstration of device capability for indentation in air and liquids.

Concerning the overall force resolution, it is important to stress that, because of mechanical vibrations, when the probe is in contact with the sample the noise at the output of the readout is generally different with respect to that measured before contact. To quantify this effect, we have fit the indentation data with a spline curve and analyzed the residuals with standard statistical algorithm. According to this analysis, the force noise of Probe-1 during indentation of PDMS 20:1, for example, is equal to  $\sim 40 \text{ nN}$  and  $\sim 60 \text{ nN}$  in air and in water, respectively. The force noise observed in water is slightly

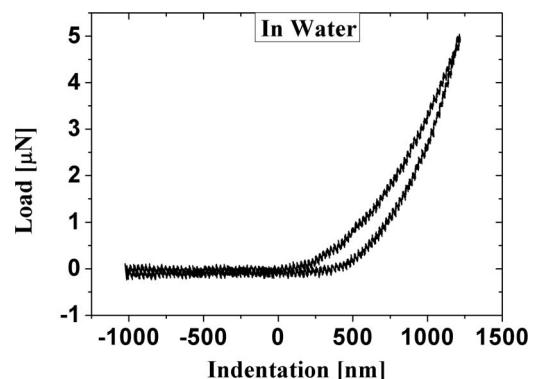


FIG. 8. Load versus indentation depth for indentation of PDMS (20:1) in liquid by Probe-1.

higher because of the effect of the capillary bridge on the side of the probe holder. This force noise can further vary for different probes and the material indented.

#### IV. CONCLUSIONS

We have presented a novel device for material property characterization. The instrument is easy to use both in air and water, and can accommodate samples of any size. The sample moduli estimated by the device when tested on a polymer sample are consistent and in good agreement with the values reported in the literature. We envision applications for *in situ* experiments and integration into other scientific instruments. Because the indenter tip is part of an optical fiber, it is feasible to develop devices where one can indent a sample while also coupling light from or to the indentation point. This opens new possibilities for simultaneous mechanical and optical characterization of materials.

#### ACKNOWLEDGMENTS

This work was supported by the European Research Council under the European Community's Seventh Framework Programme (FP7/2007-2013)/ERC Grant Agreement No. 201739, and FOM (Stichting voor Fundamenteel Onderzoek der Materie) via the Mechanosensing and Mechanotransduction by Cells program and via a Valorization Grant.

<sup>1</sup>W. C. Oliver and G. M. Pharr, *J. Mater. Res.* **7**, 1564–1583 (1992).

<sup>2</sup>M. R. VanLandingham, *J. Res. Natl. Inst. Stand. Technol.* **108**, 249–265 (2003).

- <sup>3</sup>G. Binnig, C. F. Quate, and Ch. Gerber, *Phys. Rev. Lett.* **56**, 930 (1986).
- <sup>4</sup>A. B. Mann and J. B. Pethica, *Langmuir* **12**, 4583–4586 (1996).
- <sup>5</sup>M. R. VanLandingham, J. S. Villarrubia, W. F. Guthrie, and G. F. Meyers, *Macromol. Symp.* **167**, 15–43 (2001).
- <sup>6</sup>G. Moeller and V. Domnich, *Microsc. Microanal.* **13**, 186–187 (2007).
- <sup>7</sup>S. Hengsberger, A. Kulik, and Ph. Zysset, *Eur. Cells Mater.* **1**, 12–17 (2001).
- <sup>8</sup>Y. X. Zhu, Z. X. Dong, U. C. Wejinya, S. Jin, and K. M. Ye, *J. Biomech.* **44**, 2356–2361 (2011).
- <sup>9</sup>S. E. Cross, Y. S. Jin, J. Rao, and J. K. Gimzewski, *Nat. Nanotechnol.* **2**, 780–783 (2007).
- <sup>10</sup>Q. S. Li, G. Y. H. Lee, C. N. Ong, and C. T. Lim, *Biochem. Biophys. Res. Commun.* **374**, 609–613 (2008).
- <sup>11</sup>G. Gruca, S. de Man, M. Slaman, J. H. Rector, and D. Iannuzzi, *Proc. SPIE* **7503**, PDP07 (2009).
- <sup>12</sup>D. Chavan, G. Gruca, S. de Man, M. Slaman, J. H. Rector, K. Heeck, and D. Iannuzzi, *Rev. Sci. Instrum.* **81**, 123702 (2010).
- <sup>13</sup>D. Chavan, D. Andres, and D. Iannuzzi, *Rev. Sci. Instrum.* **82**, 046107 (2011).
- <sup>14</sup>T. Pangaribuan, K. Yamada, S. Jiang, H. Oshawa, and M. Ohtsu, *Jpn. J. Appl. Phys.* **31**, 1302 (1992).
- <sup>15</sup>D. Iannuzzi, S. Deladi, V. J. Gadgil, G. P. Sanders, H. Schreuders, and M. C. Elwenspoek, *Appl. Phys. Lett.* **88**, 053501 (2006).
- <sup>16</sup>H. Hertz, in *Miscellaneous Papers* (Macmillan, London, 1896).
- <sup>17</sup>K. L. Johnson, K. Kendall, and A. D. Roberts, *Proc. R. Soc. London, Ser. A* **324**, 301 (1971).
- <sup>18</sup>B. V. Derjaguin, V. M. Muller, and Y. P. Toporov, *J. Colloid Interface Sci.* **53**, 314–326 (1975).
- <sup>19</sup>D. Tabor, *J. Colloid Interface Sci.* **58**, 2 (1977).
- <sup>20</sup>D. Maugis, *J. Colloid Interface Sci.* **150**, 243 (1992).
- <sup>21</sup>D. M. Ebenstein and K. J. Wahl, *J. Colloid Interface Sci.* **298**, 652–662 (2006).
- <sup>22</sup>J. C. Grunlan, X. Y. Xia, D. Rowenhorst, and W. W. Gerberich, *Rev. Sci. Instrum.* **72**, 2804 (2001).
- <sup>23</sup>D. M. Ebenstein, *J. Mater. Res.* **26**, 1026–1035 (2011).
- <sup>24</sup>F. Carrillo, S. Gupta, M. Balooch, S. J. Marshall, G. W. Marshall, L. Pruitt, and C. M. Puttlitz, *J. Mater. Res.* **20**, 2820–2830 (2005).